ORIGINAL PAPER

Low-cost Zeolite/TiO$_2$ composite for the photocatalytically enhanced adsorption of Cd^{2+} from aqueous solution

Najm Us Saqib[1,2,3] · Rohana Adnan[2] · Muhammad Rahim[2] · Ajmal Khan[3]

Abstract

Nano-TiO$_2$ (anatase) powders were immobilized on crystalline zeolite (size = 45 μm). The composite material was used for the rapid and efficient adsorption of the Cd^{2+} ions from an aqueous solution. Furthermore, the composites were exposed to two different calcination temperatures (500 and 700 °C) and were characterized by employing XRD, UV–Vis DRS, EDX, XRF, and pH point of zero charge analyses. Green synthesis, impregnation method was used to obtain zeolite-supported TiO$_2$. The present study demonstrated that the photocatalytic maximum adsorption capacity of Cd^{2+} by zeolite-supported TiO$_2$ (q_m = 59.3 mg/g) was 3.7 times higher than that of bare TiO$_2$ (q_m = 16.2 mg/g). The percent removal efficiency of 99.6% was observed using zeolite-supported TiO$_2$ composite under compact fluorescent light. Adsorption and kinetics studies were performed and the results obtained best fitted Langmuir adsorption isotherm and pseudo-second-order kinetics. As the wastewater containing different ionic strength, model dye Methylene Blue (MB) was used as competitive ions in the adsorption process. MB acted as photo-generated positive hole (h^+) trapper and enhanced the Cd^{2+} removal efficiency (q_m = 68.8 mg/g) further by reducing electron/hole pairs recombination rate. The easily separable composite showed high reusability by physical (high-temperature combustion) regeneration as compared to chemical (Fenton oxidation) regenerated samples.

Keywords Zeolite · Titanium dioxide · Immobilization · Cd^{2+} adsorption · Regeneration

Introduction

The non-biodegradable nature of toxic pollutants such as heavy metals creates permanent impacts on the environment. The removals of these heavy metals by efficient methods are a serious area of interest for the researchers. The main sources of toxic metal contaminations are human activities and industrial development [1]. Heavy metal (i.e., Cd^{2+}) enters the human body through contaminated foods, air, and water, which causes adverse effects on human health and damages the liver, kidney, and brain [1, 2]. Cd^{2+} can cause toxicity even at very low concentrations. The World Health Organization (WHO) drinking water threshold limit value (TLV) for cadmium is 0.005 mg/L [3]. Therefore, the removal of toxic metal ions from water and improving the quality of water to a safe level are huge area of interest. Various conventional approaches were applied recently for the removal of heavy metals from the aqueous medium such as ion exchange [4], reverse osmosis [5], chemical precipitation [6], adsorption [7], and using powder activated carbon treatment [8]. Besides the advantageous aspects of these methods, there are also some limitations in terms of cost-effectiveness and ineffectiveness toward varying concentrations of metals to be removed. The adsorption is the most attractive and effective method for the removal of heavy metals to overcome the problem of toxic sludge disposal [9].

A number of photocatalysts and adsorbents such as synthetic bentonite/polyaniline@Ni$_2$O$_3$ [10], biochar [11], ananas comosus [12], kaolinite clay nanotubes [13], fly ash [14], organo-bentonite/Co$_3$O$_4$ green nanocomposite [15], zeolite [16, 17], and lignin [18] have been reported for the removal of toxic metal ions and dyes. In recent years,

✉ Najm Us Saqib
  najm_saqib@yahoo.com

1   Department of Chemistry, University of Buner, Buner, KP, Pakistan

2   School of Chemical Sciences, Universiti Sains Malaysia, 11800 Penang, Malaysia

3   Department of Zoology, University of Buner, Buner, KP, Pakistan

semiconductor nanoparticles have become promising materials in the field of heterogeneous photocatalysis of wastewater treatment.

Titanium dioxide (TiO_2) nanoparticle is one of the excellent photocatalysts that has been studied for its successful photo-oxidations of organic compounds. In comparison with the photo-oxidation application of TiO_2 nanoparticles, the photo-reductions process got less importance. The basic reason is since the photo-generated electrons (e^-, conduction band) are relatively weaker reductant as compared to valance band photo-generated holes (h^+, valence band), which act as a strong oxidant [19]. The photo-reduction and removal of metal ions using TiO_2 nanoparticles are potentially attractive applications for the recovery of metals from industrial wastewaters as well as environmental remediation [20]. Furthermore, the immobilization of TiO_2 on inert solid substrates not only enhances the photo-activity of TiO_2 nanoparticles but also makes the nanoparticles easily separable from aqueous solutions [16, 21]. Similarly, Tayade et al. reported earlier that zeolite solid support acts as a microreactor for the TiO_2 nanoparticles and reduces the electron–hole pair recombination of catalyst, by the enhanced adsorption of oxygen on zeolite surface [22]. The chemical, photochemical, thermal inertness, and high adsorption capability of the zeolite support make it a promising contender for the nanoparticles immobilization with enhanced efficiency [16].

Previously, the reported studies on the modifications of TiO_2 photocatalyst demonstrated the shift in photo-response to longer wavelength, however, most of the practical application still required UV source of irradiation. The present study is focused on the tailoring of TiO_2 nanoparticles by a facile method of preparation in order to reduce the barrier of UV irradiation and to shift the working wavelength to the visible range of light. The zeolite-supported TiO_2 composite was applied for the removal of the Cd^{2+} ions from the aqueous solution. The kinetics and adsorption studies were conducted in normal conditions of pH (pH ~ 6.8 ± 0.2) and under compact fluorescent light. The positive hole scavengers (organic additive, MB) play an important role in reducing electron–hole pairs recombination rate, which further enhanced the efficiency to complete removal of Cd^{2+} ion from aqueous solution.

Experimental

Materials and methods

Titanium(IV) oxide, general-purpose reagent (GPR, amorphous), zeolite (size 45 μm, crystalline), and iron nitrate were purchased from Sigma-Aldrich, while cadmium nitrate, Methylene Blue, $NaNO_3$, HNO_3, and NaOH were received from QRec Asia, and calcium chloride was purchased from

R & M chemicals. All chemicals were of analytical grade and were used without further purification.

Modified liquid impregnation (LI) method was used to obtain TiO_2 nanoparticles using commercially available amorphous titanium (IV) oxide [16]. Firstly, 3 g GPR TiO_2 was slowly added to 100 mL of distilled water and the solution was allowed to mix on a magnetic stirrer (model DAIHAN WiseStirr) at a stirring rate of 350 rpm. The slurry was continuously stirred for 12 h and then allowed to settle for another 12 h. Later, the slurry was dried in an oven for 12 h at 105 °C. The dried samples were ground and calcined at different calcination temperatures (i.e., 500 and 700 °C) for 3 h in a furnace. Furthermore, a conventional impregnation process was applied to obtain zeolite-supported TiO_2 composites [23]. For the synthesis of zeolite-supported TiO_2 nanoparticles, aluminosilicate (crystalline zeolite) was used without any treatment. TiO_2 nanoparticles and crystalline zeolite were used in the ratio of 80:20%. Firstly, pure anatase TiO_2 slurry was prepared in distilled water. Secondly, the crystalline zeolites were dissolved in 100 mL of distilled water mixed with TiO_2 sol followed by vigorous stirring (400 rpm) for 3 h. The resulting mixture was kept in the oven at 110 °C for 12 h. After drying, the samples were ground properly and exposed to different calcination temperatures (500 and 700 °C) in an open-air furnace.

Characterizations

The phase composition and crystallite sizes of pure and zeolite-supported nanoparticles were investigated by the powder X-ray diffraction technique. PANalytical X'Pert PRO MRD PW3040 instrument was used to obtain XRD patterns at Cu-K$_\alpha$ radiation at $2\theta = 20°$ to $80°$. Debye–Scherrer equation (Eq. 1) [16, 24] was used to calculate the crystallite sizes:

$$D = \frac{k\lambda}{\beta \cos\theta} \tag{1}$$

where λ is the wavelength of radiation ($\lambda = 1.54$ Å), k ($= 0.9$) is the shape factor, β is the full width of half of the maximum (FWHM). The W_A weight fraction of the anatase phase is calculated using Eq. 2 [25]:

$$W_A = \frac{k_A A_A}{k_A A_A + A_R + k_B A_B} \tag{2}$$

where A_A, A_B, and A_R are the integrated intensities of the anatase (1 0 1), brookite (1 2 1), and rutile (1 1 0) peaks. The values of k_A and k_B are 0.886 and 2.721, respectively [25]. The internal surface morphology and texture of the prepared materials were studied by SEM and TEM analyses using FEI Quanta FE650 and Philips CM 12 instruments. BET surface area and porosity analyses were carried out by N_2 adsorption–desorption studies using a surface area analyzer model

ASAP 2020 V4.01. The BET surface area was calculated using nitrogen adsorption–desorption isotherm measurement at 77 K. CARY 5000 UV/VIS/NIR UV/Vis spectrophotometer was used for the diffused reflectance (UV–Vis DRS) study of zeolite-supported and pure TiO_2 samples. To calculate the indirect bandgap transition of the prepared samples, the UV–Vis DRS data are examined using the Tauc equation (Eq. 3) [26].

$$\alpha = A(hv - E_g)^{1/2} \qquad (3)$$

where α is the absorption coefficient, E_g is absorption bandgap, A is the constant, and $n^{1/2}$ for indirect bandgap transition of the material.

pH of point of zero charge (pH_{PZC}) determination

A modified pH drift method was used to investigate the pH point of zero charges (pH_{PZC}) of pure and zeolite-supported TiO_2 nanoparticles [16]. The pH of the solutions (pH ~ 2, 4, 6, 8, 10, and 12) was adjusted using either 0.01 M HNO_3 or NaOH. Furthermore, 0.1 g of pure and zeolite-supported TiO_2 powder was added and equilibrated for 24 h, and the final pHs of the solutions were calculated. Initially, pre-adjusted pHs were plotted against the difference between the initial and final pH (ΔpH). For each sample, the pH values that cross the zero points of the curve were taken as the pH_{PZC} of the material.

Photocatalytic study

Working solutions of Cd^{2+} ion were prepared in deionized water using $Cd(NO_3)_2 \cdot 4H_2O$. The removal efficiency of Cd^{2+} was determined using 0.1 g of sorbent, the natural pH of the solution (pH ~ 6.8 ± 0.2), and under compact fluorescent light. All the solutions were equilibrated using an IKA Basic 260, orbital shaker for 3 h at a stirring rate of 250 rpm. To separate the nanoparticles from the aqueous medium, the suspensions were centrifuged at 5000 rpm for 5 min, while the supernatant was preserved with a few drops of 1 M HNO_3 solution. Perkin Elmer AAnalyst 400, atomic absorption spectrometer (AAS), was used to analyze the remaining concentration of Cd^{2+}.

To study the effect of pH on the removal of Cd^{2+}, a series (pH ~ , 6, natural pH (6.8 ± 0.2), 8 and 10) of 80 mL solutions (100 mg/L) of Cd^{+2} were prepared. The pH was adjusted using either 0.01 M HCl or NaOH. As much as, 0.1 g of the sorbent was added and after a predetermined time interval, the mixture was centrifuged and tested for the remaining Cd^{+2} concentration. The effect of organic additive (MB) on the adsorption of Cd^{2+} was evaluated at native pH and under compact fluorescent light. The competitive study was performed using binary solutions of MB (200 mg/L)

and Cd^{2+} (200 mg/L). The remaining amount of Cd^{2+} and dye (MB) were analyzed using a Perkin Elmer AAnalyst 400 atomic absorption spectrometer and Shimadzu 2600 UV–VIS spectrophotometer, respectively.

Kinetic study

The kinetic studies were carried out using 250 mL flasks. For each test, 0.1 g zeolite-supported and pure TiO_2 nanoparticles were used in 80 mL of 100 mg/L Cd^{2+} solutions. The solution was agitated at 250 rpm while collecting the samples at regular time intervals. The collected samples were centrifuged for 5 min operated at 5000 rpm. The concentration of residual Cd^{2+} was analyzed using AAS. The photocatalytic removal capacity of all as-prepared catalysts was calculated from the amount of Cd^{2+} adsorbed using the mass balance equation as:

$$qt = \frac{(C_o - C_t)V}{m} \qquad (4)$$

where C_o and C_t are the initial Cd^{2+} concentration (mg/L) and the Cd^{2+} concentration at any time t, respectively. V is the volume (mL) of Cd^{2+} solution, and m is the weight of nanoparticles.

Adsorption study

The adsorption efficiency of zeolite-supported and pure TiO_2 samples was carried out in batch mode using 100 mL flasks. The batch test was performed using 80 mL of Cd^{2+} solutions of different concentrations (10, 20, 30, 60, 100, and 150 mg/L) that were mixed with 0.1 g with zeolite-supported and pure TiO_2 nanoparticles. The orbital shaker with a speed of 260 rpm was used for 3 h to ensure complete adsorption. Isotherm experiments were performed with different initial Cd^{2+} concentrations at room temperature, 25 °C. The contact time was kept at 3 h, and the native pH of Cd^{2+} solutions was chosen as the experimental conditions.

Regeneration study

The regeneration study of the used samples was carried out by high-temperature combustion and Fenton oxidation (FR) methods, with slights alterations [27]. In the high-temperature combustion method, the used zeolite-supported and pure TiO_2 were exposed to high calcination treatment (530 ± 20 °C) in a furnace with a heating rate 5 °C/min for 3 h. In the Fenton oxidation method, 10^{-2} M Fe and 3% H_2O_2 solutions were prepared from $Fe(NO_3)_3 9H_2O$ and H_2O_2. The spent samples and $Fe(NO_3)_3 9H_2O/H_2O_2$ solutions were mixed for 8 h, at ambient temperature. After that, the samples were collected and washed properly with distilled

water. For collecting the powder nanoparticles, all the samples were centrifuged for 5 min at the speed of 5000 rpm. After centrifugation, the samples were dried at 110 °C, in an oven. Regeneration of used samples was performed three times.

Desorption study

The desorption study of the adsorbed Cd^{2+} ions from zeolite-supported and pure TiO_2 was performed to validate the effective adsorption process. Used samples of kinetics experiments at 100 mg/L Cd^{2+} solutions were washed properly with distilled water to remove un-adsorbed Cd^{2+} ions. The samples were dried at 60–70 °C in an oven. The dried samples were added to 0.01 M $CaCl_2$ solutions in separate flasks and shaken for 3 h [1]. To measure the desorbed equilibrium concentration of Cd^{2+} ions, the solutions were centrifuged for 5 min at 5000 rpm speed and the supernatant collected was analyzed using AAS.

Results and discussions

Characterizations

The crystallite sizes of materials calcined at different temperatures were calculated using Scherrer equation (Eq. 1) for anatase (1 0 1) peak and percentage composition of anatase phase using Eq. 2, and the values are given in Table 1. The diffraction peaks at angles (2θ) 24°, 26.5°, and 31.2° (Fig. S1) are corresponding to the diffraction peaks of Faujasite-Na [28]. Similarly, the disappearance of zeolite (aluminosilicate) broad peaks (at $2\theta = 20–35°$) is due to overlap with the typical anatase TiO_2 diffraction peak (25.28°) and also the zeolite surfaces are covered with nanoparticles [16, 28]. Pure TiO_2 XRD pattern reveals the presence of only anatase phase and no rutile or brookite reflections were observed. However, in zeolite-supported TiO_2, brookite and rutile peaks reflections are obvious, as shown in Fig. 1. The high calcination treatments (700 °C) did not change the peak position of zeolite or TiO_2, indicating that the zeolite has good thermal

stability and revealing that most of the zeolite surface was covered with TiO_2 nanoparticles.

Surface area and pore sizes of metal oxide nanoparticles are of utmost importance to specify the photocatalytic activity of the nanoparticles. An increase in the surface area directly enhances the photocatalytic efficacy. Brunauer–Emmett–Teller (BET) surface areas and Barrett-Joyner-Halenda (BJH) pore size distributions of all the prepared nanoparticles were calculated from nitrogen adsorption–desorption isotherms. The reduction in the surface areas was observed for the zeolite-modified samples compared to pure TiO_2, due to the larger sizes of zeolite support materials (zeolite surface area = 4.2 m^2/g), Table 1. As the heterostructures consist of a 4:1 ratio of TiO_2 and solid support, most of their porosity texture is similar to and controlled by TiO_2 nanoparticles (precursor). The prepared nanocomposite samples exhibited a type-IV hysteresis loop (Fig. S2).

The anatase phase of TiO_2 is an indirect bandgap semiconductor [29]. Therefore, for indirect electronic transition, the bandgap energy (E_g) of zeolite-supported and pure TiO_2 was calculated from the plot of $(\alpha hv)^{1/2}$ versus photon energy (E_g, eV) (Fig. 2), and the values are given in Table 1. A previously reported study indicated that the zeolite@TiO_2 shows poor absorption in the visible (400–800 nm) region [28]. However, in the present study, the zeolite-supported TiO_2 revealed photo-response shifted to longer wavelength (visible region) and bandgap energy of composites reduced to 2.90 eV (from 3.20 eV of pure TiO_2). The possible reason for the longer wavelength shift (visible shift) is due to the uniform dispersion of TiO_2 nanoparticles on the zeolite surface, prepared by the physical impregnation (LI) method. Similarly, our previous finding [16], FTIR results also indicated that there is no chemical interaction exists between zeolite support and TiO_2 nanoparticles prepared by the LI method. The non-appearance of chemical bonding could be the possible reason for the absorption of zeolite-supported samples in the visible region. The XRD results also indicated that the major part of nano-sized TiO_2 is present on the surface of the zeolite. The coupling effect of zeolite and TiO_2 is responsible for the narrowing of the bandgap of zeolite-supported TiO_2 as compared to pure TiO_2.

Table. 1 Crystallite sizes, the percentage phase composition, $pH_{PZC,}$ and bandgap energy of pure and zeolite-supported TiO_2 nanoparticles

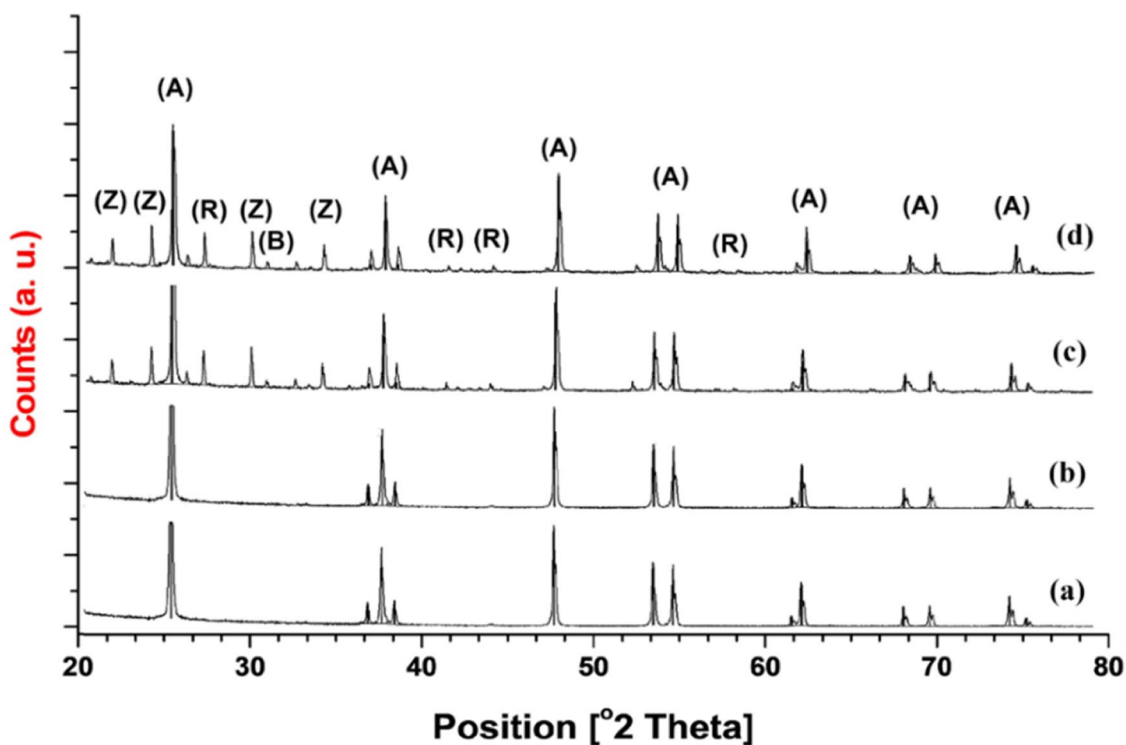| NPs		Calcinations temperature (°C)	Anatase phase (%)	Rutile and Brookite (%)	Anatase (1 0 1) crystallites size(nm)	Average crystallites size (nm)	Bandgap (eV)	Surface area (m^2/g)	Pore volume (nm)
TiO_2	T-5	500	100	–	55.7	56.8	3.15	10.7	12.1
	T-7	700	100	–	55.6	64.0	3.18	9.11	12.3
Z@TiO_2	ZT-5	500	86	14	55.7	58.3	2.91	7.30	13.2
	ZT-7	700	85	15	55.7	76.6	2.90	6.63	13.5

Fig.1 XRD patterns of **a** TiO$_2$-500 °C, **b**TiO$_2$-700 °C **c** zeolite-supported (ZT-5) 500 °C and **d** 700 °C (ZT-7), respectively. (A = Anatase phase, R = Rutile phase, B = Brookite phase, Z = Zeolite)

The morphological studies of the prepared materials analyzed by SEM are given in Fig. 3. It can be observed from the SEM images that the zeolite-supported TiO$_2$ exhibited uniform distribution of spherical nanoparticles on the surface of the solid supports. The SEM results indicate that the average particle sizes of TiO$_2$ nanoparticles are less than 0.1 μm. The effects of calcination treatment seem to be significant in the zeolite-supported samples, where is the agglomerations of TiO$_2$ nanoparticles on the solid support surface are comparatively higher for 500 °C calcined sample than the sample calcined at 700 °C. Though, the dispersion of nanoparticles is more uniform on the surface of zeolite for samples calcined at the lower temperature (500 °C). The pure TiO$_2$ nanoparticles form agglomerates at both calcination treatments, which could reduce the active surface area and the probable reason for the reduction in efficiency. The TEM micrographs given in Fig. 4 show that the average particle sizes of TiO$_2$ are in the range of 60–90 nm. However, the zeolite particles in zeolite-supported samples tend to undergo agglomeration to form larger particles at higher calcination temperature (700 °C), and the sizes of zeolite support reach more than 200 nm. The TEM images of zeolite-supported samples calcined at 500 and 700 °C showed a uniform dispersion of spherical shape TiO$_2$ nanoparticles around the zeolite particles. The SEM and TEM particle sizes of TiO$_2$ were observed larger than the sizes calculated

from the Scherrer equation, which can be due to the presence of agglomerates formed due to the high surface energy of the TiO$_2$ particles [30].

The charge associated with the metal oxide semiconductors surface functionality plays a vital role in heterogeneous photocatalysis. In the heterogeneous reactions, the proper pH selections can alter the surfaces of the photocatalysts for the uptake of anionic or cationic pollutants. The pH of the point of zero charges is the point where the net surface charge of materials is zero and is known as the pH$_{PZC}$ [16]. The pH$_{PZC}$ of TiO$_2$ nanoparticles mainly depends upon several factors such as chemical modifications of the surface, particle size, and phase transformation [31]. pH drift method results for pH$_{PZC}$ of zeolite-supported and pure TiO$_2$ are given in Table 2. For zeolite-supported and pure TiO$_2$ samples, at pH < pH$_{PZC}$, the TiO$_2$ surface has a net positive charge, whereas at pH > pH$_{PZC}$, the surfaces are negatively charged. However, the presence of zeolite support increases the surface positivity and negativity of charges at different pH as compared to pure TiO$_2$, Fig. 5(a).

Effects of pH on the adsorption of Cd^{2+} ions

The pH of solutions strongly influences the surface charge, particle size, and the absorption band edges position of TiO$_2$, it also controls the protonation state of the surface
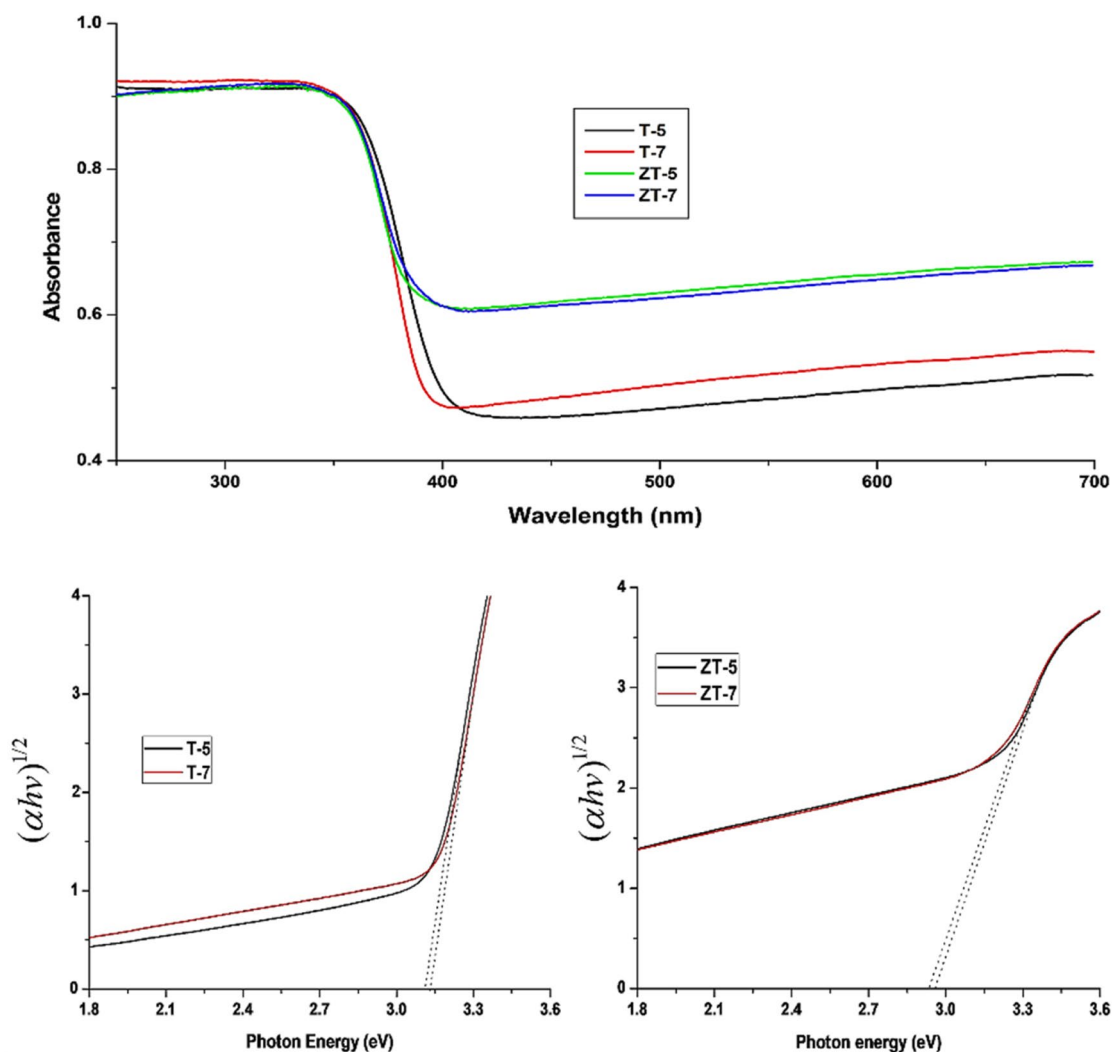
Fig. 2 Absorbance and Tauc plot for pure and zeolite-supported TiO$_2$ nanoparticles calcined at different temperatures

hydroxyl groups on TiO$_2$ photocatalyst. The effects of pH were observed pronounced on the size of semiconductor aggregates, and aggregation was found more obvious at pH$_{PZC}$ [16].

The effects of change in pH were evaluated for the adsorption of Cd^{2+} ions using zeolite-supported and pure TiO$_2$, Fig. 5(b). The working pH of the solutions (4, 6, native pH of the solution, 8 and 10) was selected on the base of pH$_{PZC}$ of the materials. The effective adsorption of Cd^{2+} ions from the solutions shows the variation in efficiencies for the as-prepared zeolite-supported and pure TiO$_2$ samples. The pure TiO$_2$ samples show the removal intensity trend, increasing from lower (4 to 6) to higher pH until reaches the maximum at pH 10, Table 2. However, zeolite-supported 500 °C calcined sample shows merely same adsorption on the all selected pH (i.e., 4,6, neutral pH of the solution, 8 and 10), while 700 °C calcined sample has maximum adsorption at pH 7. The increasing of pH decreases the solubility of

metals and the metal ions tend to form precipitates. Similarly, Samarghandi et al. observed that 69.5% of Cd^{2+} was removed from the solution at higher pH (pH = 11) without adding any adsorbent [32]. Hence, it is apparent from previously reported results that working at higher pH for the removal of metal ions did not show the significant effectiveness of adsorbents. In the present study, it was observed that Cd^{2+} ions precipitated in the absence of photocatalyst materials at pH above 7 and the maximum precipitation of ~50% were recorded at pH 10, (Fig. 5(b) (Blank)).

Competitive adsorption study

In the photocatalytic processes, oxidation and reduction occur simultaneously. The organic additives are often used as hole scavengers, however, in the absence of oxidants, water molecules are photo-oxidized [16, 20, 33]. Organic additive enhances the photocatalytic activity by following
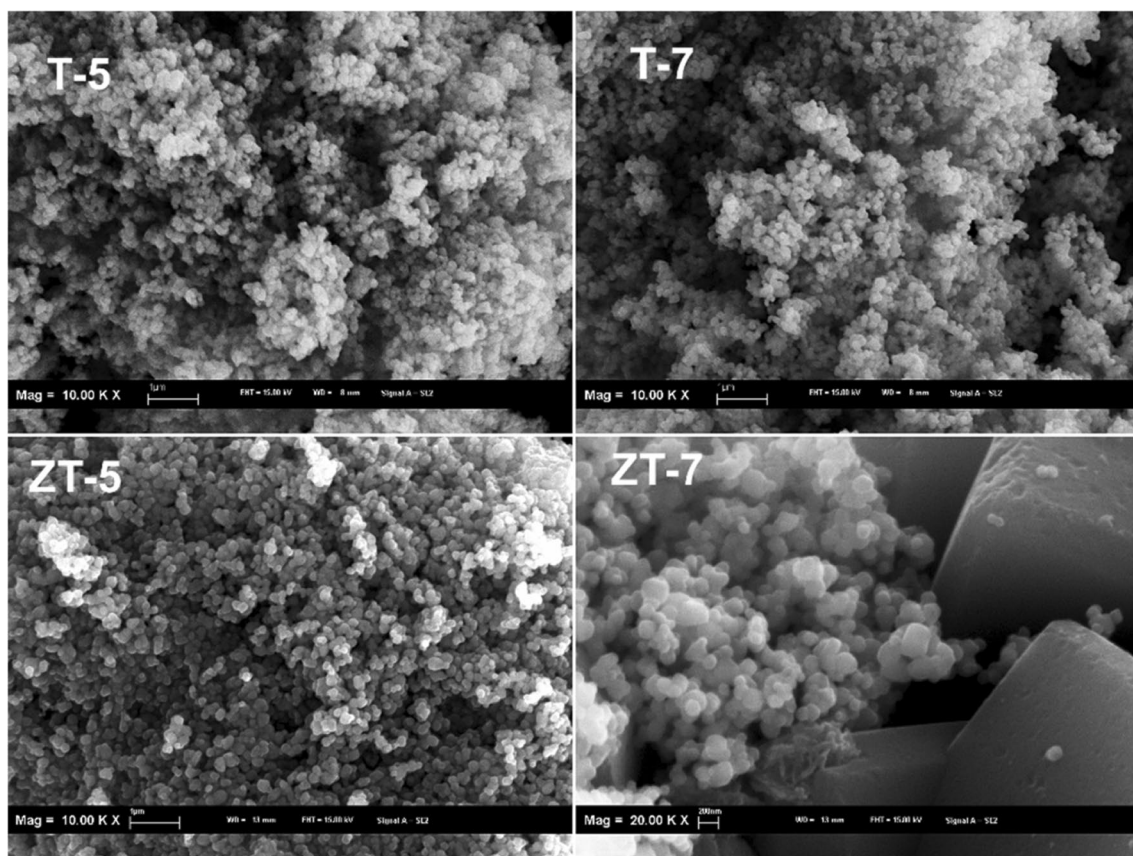
Fig. 3 SEM images of pure and zeolite-supported TiO_2 nanoparticles

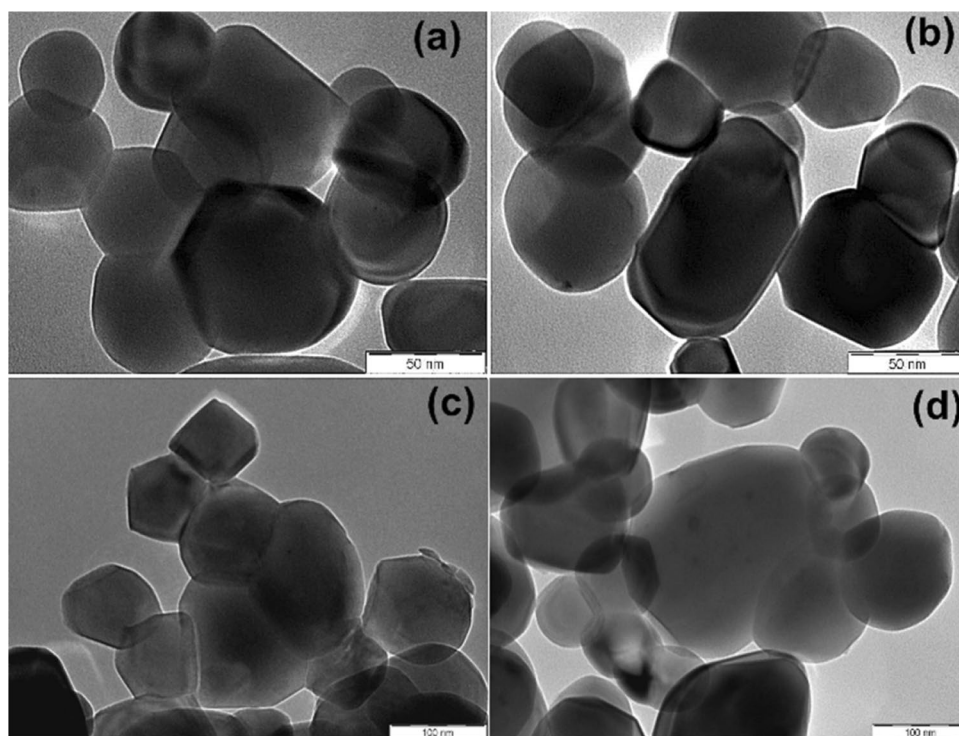**Fig. 4** TEM images of **a** T-5, **b** T-7, **c** ZT-5, and ZT-7

Table. 2 Maximum adsorption capacity, q_t (mg/g) of Cd²⁺ (100 mg/L) removal for different pH

NPs	pH$_{(PZC)}$	Cd²⁺ adsorption capacity, q_t (mg/g) at pH				
		4	6	Native pH of solution (6.8 ± 0.2)	8	10
T-5	6.6	17.6	20.8	16.0	31.2	39.7
T-7	7.0	16.8	20.0	14.2	30.1	39.5
ZT-5	7.4	39.9	39.8	39.9	39.9	40.0
ZT-7	7.8	39.0	38.9	39.8	39.9	40.0

Fig. 5 **a** pH point of zero charge for pure TiO₂ and zeolite-supported TiO₂ by pH drift method, and **b** the effects of various pH on adsorption efficiency of Cd²⁺ on to pure TiO₂ and zeolite-supported TiO₂
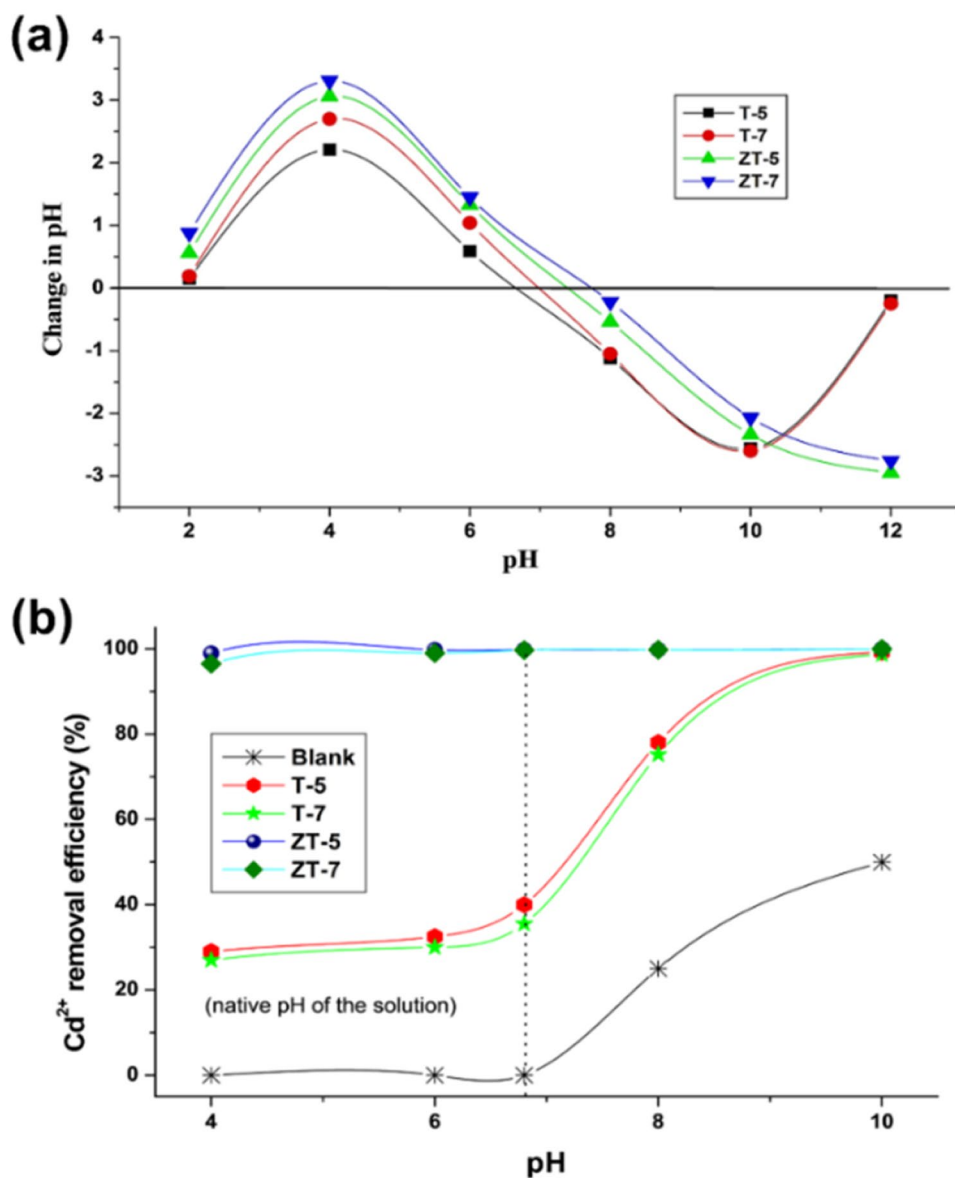
four possible ways, (i) enhancing metal ions adsorption on the surface of photocatalyst, (ii) modifying the reduction potential of metal after complexation, (iii) modifying the redox properties of TiO₂ photocatalyst, and (iv) improving the charge separations [20, 33]. The photo-generated electrons and holes of the semiconductor mechanism follow the transfer of an electron to sorbed metal ions while the holes oxidize the scavenger present in the solution. The electron transfer occurs via two-step electron transfer which reduces the metal (Cd²⁺) from +2 valance state to into an elemental state [20, 34].

To understand the reduction mechanism of heavy metals using TiO$_2$ nanoparticles, the competitive studies with the organic compounds are found very best. The presence of the organic molecule (i.e., MB) shows the enhanced adsorption of Cd^{2+} ions from solution by all as-prepared zeolite-supported and pure TiO$_2$ photocatalysts, Table 3.

The present study using basic dye (MB) as an electron scavenger revealed that the mechanism follows the photo-induced reduction of Cd^{2+} ions using pure and zeolite-supported TiO$_2$ nanoparticles. Evidence of organic additive acting as positive hole (h^+) scavenger is explained from the obtained results of competitive adsorption study. The organic additive plays an important role to trap positive holes (h^+) and hence reducing photo-generated electron–hole pairs recombination rate, resulting in enhancement of photo-activity. Present results show that without using MB in solution, the maximum removal efficiency for Cd^{2+} adsorption by TiO$_2$ 500 °C and 700 °C reached ~40% after

3 h under compact fluorescent light. However, in presence of MB, the removal efficiency for the adsorption of Cd^{2+} ions reached ~97% after 3 h under the same set of conditions. Similarly, for the degradation of MB while using TiO$_2$ 500 °C and 700 °C without competitive (Cd^{2+}) ion, the efficiency was observed to be 10 and 9.3%, respectively, after 3 h under the same conditions. In presence of Cd^{2+} ions, the degradation efficiency of MB enhanced to 48 and 42.6%, respectively. The zeolite-supported 500 °C calcined sample shows almost complete removal for Cd^{2+} and MB after 3 h under compact fluorescent light. Besides, the efficiency of zeolite-supported 700 °C calcined sample also shows effective enhancement and reaches the values of 99.8 and 98.8% removal for Cd^{2+} and MB, respectively.

Cd^{2+} adsorption in the dark and contact time study

The adsorption in the dark and photo-induced adsorptions of Cd^{2+} onto pure and zeolite-supported TiO$_2$ under compact fluorescent light are given in Fig. 6. The dark adsorption study indicated that the zeolite-supported TiO$_2$ nanoparticles showed higher adsorption (500 °C = 25 and 700 °C = 23 mg/L) as compared to pure TiO$_2$ nanoparticles (500 °C = 9 and 700 °C = 5 mg/L). As the pH$_{PZC}$ (near to or greater than pH 7) of all the prepared samples is close to the pH of Cd^{2+} native solutions (~6.8), and the surface charges were more positive at pH < 7, hence decrease in the adsorption on the positive surface was detected. It is assumed that the higher adsorption in the dark for zeolite support TiO$_2$ nanoparticles was due to the zeolite support. Hence, the

Table.3 Maximum adsorption capacity, q_t (mg/g), of Cd^{2+} and MB (for Cd^{2+}:MB concentration 200:200 mg/L) on to zeolite-supported and pure TiO$_2$

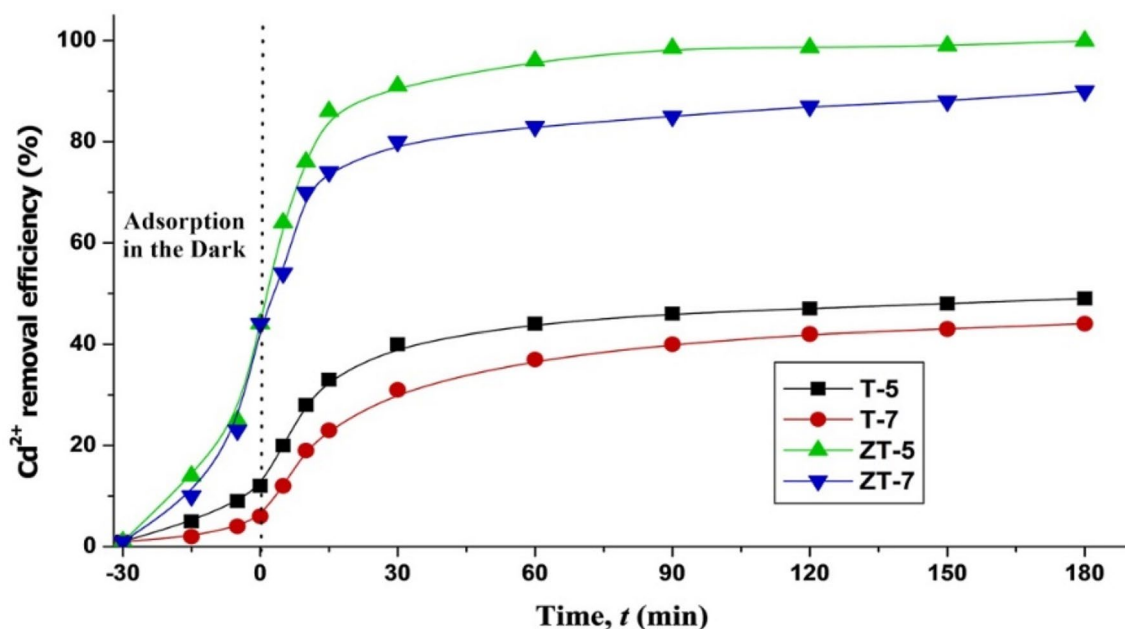| NPs	Cd^{2+}:MB (mg/L)	Cd^{2+}, q_t (mg/g), without MB	Cd^{2+}, q_t (mg/g), with MB	MB, q_t (mg/g)
T-5	100:100	16.2	27.2	28.8
T-7		14.6	28.8	25.6
ZT-5	200:200	59.3	68.8	68.0
ZT-7		54.6	61.8	60.9

Fig. 6 Adsorption in the dark and equilibrium study of the adsorption of Cd^{2+} (100 mg/L) on to zeolite-supported and pure TiO$_2$

presence of zeolite as support materials can significantly overcome the restriction of light photons, which are the requirement of photocatalyst activations.

The contact time study was investigated for the removal of the Cd^{2+} ions to evaluate the optimum contact time for Cd^{2+} ions adsorption from the aqueous solution. Figure 6 shows that the rapid adsorption of Cd^{2+} ions can be seen in the first 60 min and the equilibrium is established in the first hour. The further increase in contact time shows a very low significant increase in adsorption. Therefore, the first 60 min was selected as the optimum contact time for all the zeolite-supported and pure TiO_2 nanoparticles. The removal efficiency of zeolite-supported TiO_2 samples is much higher as compared to pure TiO_2.

Kinetics study

The kinetics study of Cd^{2+} adsorption was performed for all the as-prepared zeolite-supported and pure TiO_2 nanoparticles, and the kinetics parameters are listed in Table 4. Pseudo-first order, pseudo-second-order, and intraparticle diffusion models were applied to the data in order to understand the adsorption mechanisms of the materials. The pseudo-second-order kinetic model equation is generally expressed as reported in the literature [35]:

$$\frac{t}{q_t} = \frac{1}{k_2 q_2^2} + \left(\frac{1}{q_2}\right)t \tag{5}$$

where q_2 is the maximum adsorption capacity (mg/g) and k_2 (g/mg min) is the rate constant of pseudo-second-order for the degradation process. The plots between q_t versus t for zeolite-supported and pure TiO_2 are shown in Fig. 7. The adsorption curve best fitted to the pseudo-second-order model, with a correlation factor (R^2), values more than 0.97, indicating the adsorption is close to chemisorptions. Pseudo-first-order kinetics was also applied on obtained data, which shows the correlation coefficients (R^2) are much lower (0.74–0.92) as well as the deviations of calculated and experimental maximum adsorption capacity, q_e (mg/g) is too high. On the contrary, the pseudo-second-order kinetics best fitted to the obtained experimental results.

In order to evaluate the mechanism of Cd^{2+} ions adsorption onto zeolite-supported and pure TiO_2 nanoparticles, the intraparticle diffusion model was also applied (Eq. 6) [36].

$$q_t = k_P t^{1/2} + I \tag{6}$$

where k_P (mg/g $min^{1/2}$) is the rate constant of intraparticle diffusion and I is the intercept of the line (mg/g) which is proportional to the boundary layer thickness. The intraparticular diffusion rate constant and intercept were calculated from the plot of q_t versus $t^{1/2}$, as shown in Fig. 7. When the plot is a straight line and it passes through the origin, then the intraparticle diffusion is a rate-controlling step, while if the plot is nonlinear or linear and does not pass through the origin, then chemical reaction or the film diffusion controls the adsorption rate [37]. By the plots of q_t versus $t^{1/2}$ of Cd^{2+} ions adsorptions data, two stages of adsorption were observed. Figure 7 indicates the first sharper portion attributed to the adsorption of Cd^{2+} ions from the solutions to the external surface of adsorbents. The second portions of the curve indicate the gradual adsorption stage, where the intraparticle diffusion is the rate-limiting step [36]. In Table 4, the kinetic parameter of the intraparticle diffusion model is presented.

EDX analysis

The elemental compositions obtained from EDX and XRF analyses of selected (500 °C) fresh and spent samples are given in Table 5. The used sample results showed the presence of cadmium on the surface. The carbon presence may be due to the carbon tape (adhesive) used during sample preparation. The surface contents observed from EDX and XRF results of pure and zeolite-supported TiO_2 showed the major component of TiO_2, along with Na, Al, and Si presence in zeolite-supported TiO_2. The spent catalysts EDX and XRF results illustrate the presence of adsorbed Cd^{2+} in significant amounts. The concentration of Cd^{2+} on the surface of pure TiO_2 is considerably low as compared to zeolite-supported TiO_2 nanoparticles (Table 5).

Table. 4 Kinetics parameters of the photocatalytic adsorption of Cd^{2+} ions by zeolite-supported and pure TiO_2 at 25 °C

NPs	Pseudo-second-order				Intraparticle diffusion					
	$q_{m,}$ exp (mg g^{-1})	$q_{m,}$ cal (mg g^{-1})	k_2, 10^{-3} (g/ mg min)	R^2	Kp		I		R^2	
					Kp1	Kp2	I1	I2	$R^2$1	$R^2$2
ZT-5	39.6	40.0	0.063	0.98	4.27	0.24	15.4	37.7	0.91	0.85
ZT-7	36.0	37.0	0.067	0.99	3.39	0.48	15.0	29.4	0.92	0.99
T-5	20.0	17.8	0.174	0.97	2.13	1.43	5.50	9.30	0.95	0.97
T-7	16.0	19.0	0.166	0.98	2.20	1.32	4.20	8.40	0.98	0.95

Fig. 7 The plot of pseudo-second-order kinetics and intraparticle diffusion modeling of Cd^{2+} adsorption onto zeolite-supported and pure TiO_2
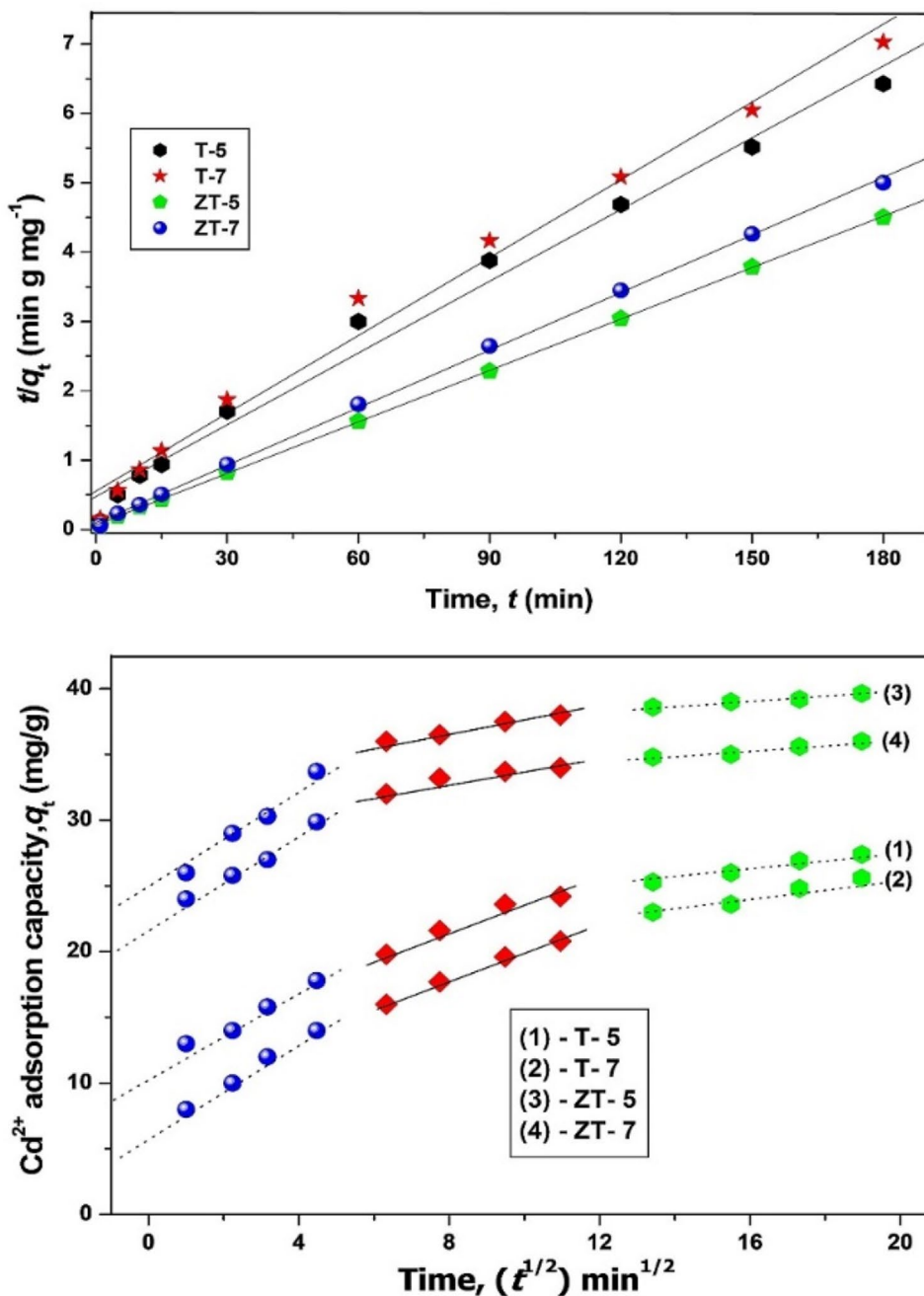

Table. 5 EDX and XRF analyses results of fresh and spent zeolite-supported and pure TiO_2 nanoparticles calcined at 500 °C

NPs	EDX mass (%)							XRF mass (%)						
	Ti	O	Al	Na	Si	Cd	C	Ti	O	Al	Na	Si	C	Cd
TiO_2 (fresh)	58.1	41.2	–	–	–	–	0.6	56.3	42.5	–	–	–	0.73	0.00
TiO_2 (used)	51.3	47.4	–	–	–	0.53	1.1	57.8	39.1	–	–	–	0.67	0.23
$Z@TiO_2$ (fresh)	50.5	40.3	2.9	2.5	3.1	–	2.2	38.6	46.1	5.0	4.7	4.3	0.75	0.00
$Z@TiO_2$ (used)	46.2	42.1	2.4	1.9	2.9	1.24	0.5	39.9	43.9	4.9	3.0	4.2	0.82	1.43

Adsorption isotherm study

To determine the adsorption capacity of Cd^{2+} ions from the solution, Langmuir isotherm was applied to the adsorption data. Zha et al. showed that for the monolayer surface adsorption which occurs on specific homogeneous sites and no interaction exists between the pollutants itself, the Langmuir model is very best suitable [38]. Hence, the Langmuir model is based on the assumptions of a structurally homogenous adsorbent and is described by the following reported equation [39]:

Table. 6 Langmuir constants of Cd^{2+} adsorption by zeolite-supported and pure TiO_2 nanoparticles at 25 °C ± 2

NPs	q_m, exp (mg/g)	q_m, cal (mg/g)	b	R_L	R^2
ZT-5	59.3	58.8	0.002	0.75–0.97	0.998
ZT-7	54.6	55.2	0.002	0.74–0.97	0.999
T-5	16.2	17.8	0.174	0.05–0.36	0.979
T-7	14.6	15.6	0.166	0.05–0.36	0.995

$$\frac{C_e}{q_e} = \frac{C_e}{q_m} + \frac{1}{q_m b} \tag{7}$$

where q_e (mg/g) is the amount of Cd^{2+} adsorbed per unit weight of adsorbents at equilibrium, C_e (mg/L) is the equilibrium concentration, q_m (mg/g) is the maximum adsorption at monolayer coverage, and b (L/mg) is the Langmuir constant related to the energy of adsorption which quantitatively shows the affinity of binding sites. The Langmuir parameters, q_m and b, were calculated from the slope and intercept of the graphs and are depicted in Table 6 and Fig. 8.

The dimensionless constant separation factor or equilibrium parameter R_L is an essential characteristic of the Langmuir isotherm model [40], which is given as follows:

$$R_L = \frac{1}{1 + bC_\circ} \tag{8}$$

where b (L/mg) is Langmuir constant, and $C_\circ$ (mg/L) is the initial concentration. The R_L value has been classified as $R_L > 1$, $0 < R_L > 1$, and $R_L = 0$, suggesting that adsorption is
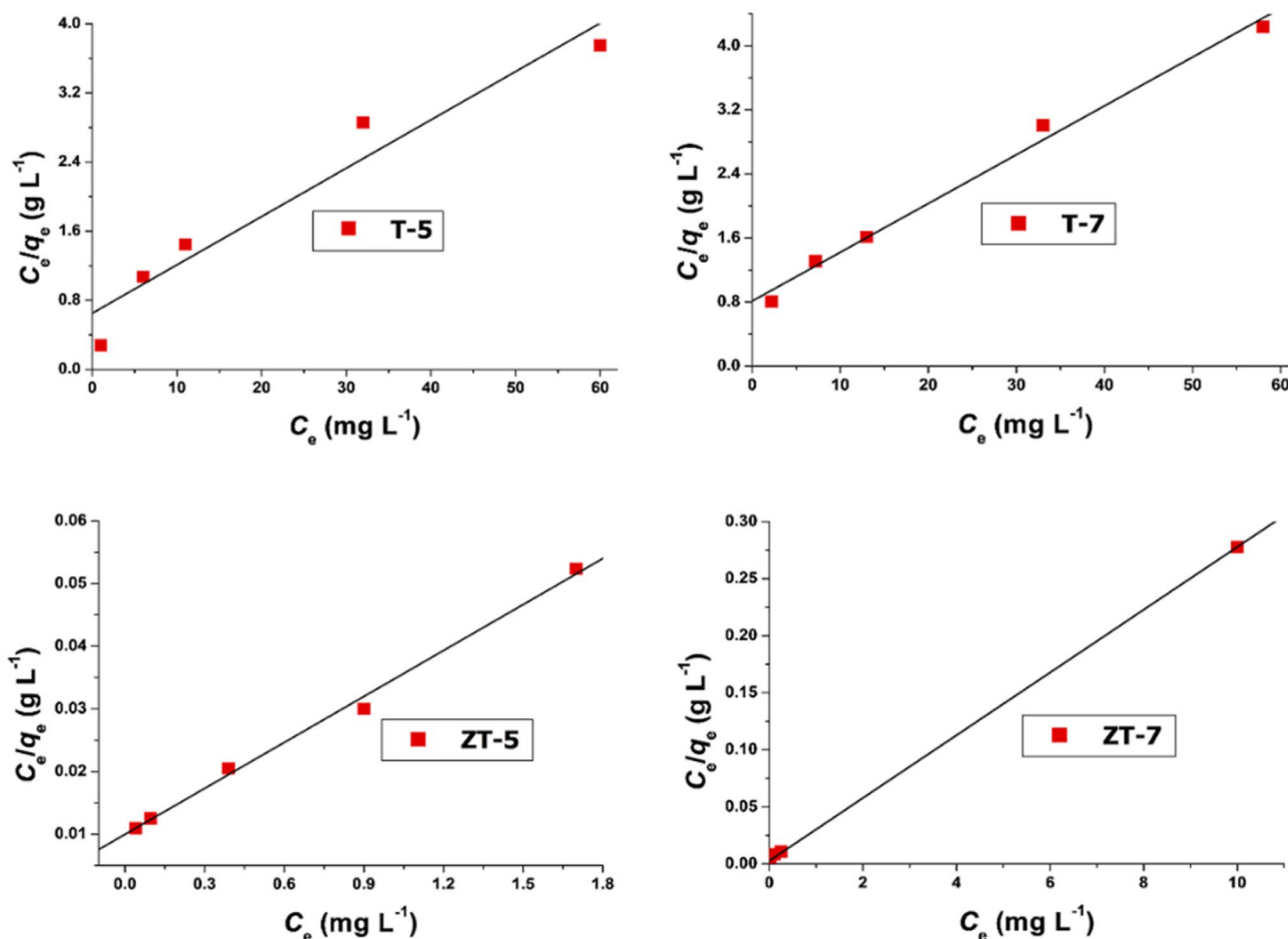

Fig. 8 Fitting plots for the Langmuir isotherm model of Cd (II) adsorption

unfavorable, favorable, and irreversible, respectively [40]. The R_L values calculated for Cd^{2+} ions adsorption are less than unity showing the favorable adsorption (Table 6). The experimental results well fitted to the Langmuir model and the monolayer maximum adsorption capacities (q_m) of Cd^{2+} ions reached 59.3 and 54.6 mg/g for zeolite-supported 500 °C and 700 °C calcined samples, respectively.

In comparison with the previously reported studies with different adsorbents (listed in Table 7), it is obvious that zeolite-supported TiO_2 in present work shows much higher efficiency for the adsorption of Cd^{2+} ions from aqueous solutions. Therefore, the zeolite-supported TiO_2 nanoparticles are very capable of the removal of Cd^{2+} ions from water. The residue amount of Cd^{2+} ions (150 mg/L) solutions from the AAS result is 1.5 mg/L, for 500 °C calcined zeolite-supported TiO_2 (500 °C). However, approximately a complete removal of Cd^{2+} ions by zeolite-supported TiO_2 was obtained from the competitive adsorption with MB, Table 3. Hence, these results indicate that the zeolite-supported TiO_2 is equally effective for the removal of Cd^{2+} ions, in high as well as for low concentrations under compact fluorescent light.

Regeneration study

Figure 9 shows the comparison of percent adsorption efficiency of fresh and regenerated zeolite-supported and pure TiO_2 photocatalysts by high-temperature combustion and Fenton oxidation processes. As shown, the physical treatment regenerated samples exhibited high adsorption capacity than that of regenerated by chemical method. The three times regenerated samples showed lower adsorption capacity than the fresh samples, and the reduction in adsorption is more than 30%, except for the first cycle regenerated samples of zeolite-supported TiO_2. Zeolite-supported catalysts regenerated by high-temperature combustion samples in the first regeneration show similar adsorption capacity compared to that of the fresh samples; however, at second and third regeneration, the adsorption capacity reduced by 35 and 45%, respectively.

It is assumed that at high-temperature regeneration, the adsorbed Cd^{2+} ions may also cause a synergistic/doping effect with zeolite-supported TiO_2 during first cycle regeneration, which probably is the reason to give similar adsorption activity to the fresh samples. However, for the second and third cycles, the active sites/pores were hindered by a higher concentration of adsorbed Cd^{2+} ions, hence reducing the further uptake of ions. The Fe ions from the solution can be adsorbed on the surface pores of the adsorbents in the Fenton oxidation process, which might considerably reduce the ions exchange capacities of the regenerated catalyst for the re-adsorption process [27].

Table.7 Comparative adsorption capacity (mg/g) of the present work with various sorbents reported for the Cd^{2+} adsorption

Adsorbents	Adsorption capacity for Cd^{2+} (mg/g)	Competitive adsorption capacity for Cd^{2+} (mg/g)	Ref
Biochar	31.9		[11]
TiO_2-sewage sludge	29.2		[37]
Nano-TiO_2	15.2		[41]
Ananas comosus	18.2		[12]
Modified kaolinite clay	41		[42]
Mixture of fly ash and TiO_2	9.5		[14]
Fly ash	16.7		
Lignin	25.4		[18]
TiO_2-graphene oxide	14.9		[43]
Turkish coffee grounds	1.32		[7]
Sludge from a natural stabilization pond (biosorbent)	11.5		[44]
Polymer clay (Kaolin-PVA)	26.6		[45]
(Kaolin-PCL)	12.1		
Date palm biochar (BC-300)	26.9		[46]
(BC-700)	43.5		
TiO_2-humic acid	9.9	19.3	[1]
TiO_2-walnut shell	25.7	9.9	
TiO_2-carbazon	31.7	14.4	
T-5	16.2	27.2	Present
T-7	14.6	28.8	Study
ZT-5	59.3	68.8	
ZT-7	54.6	61.8	

Fig. 9 Comparison of maximum removal capacity, q_t (mg/g), of Cd^{2+} (100 mg/L) on fresh and regenerated zeolite-supported and pure TiO_2 nanoparticles
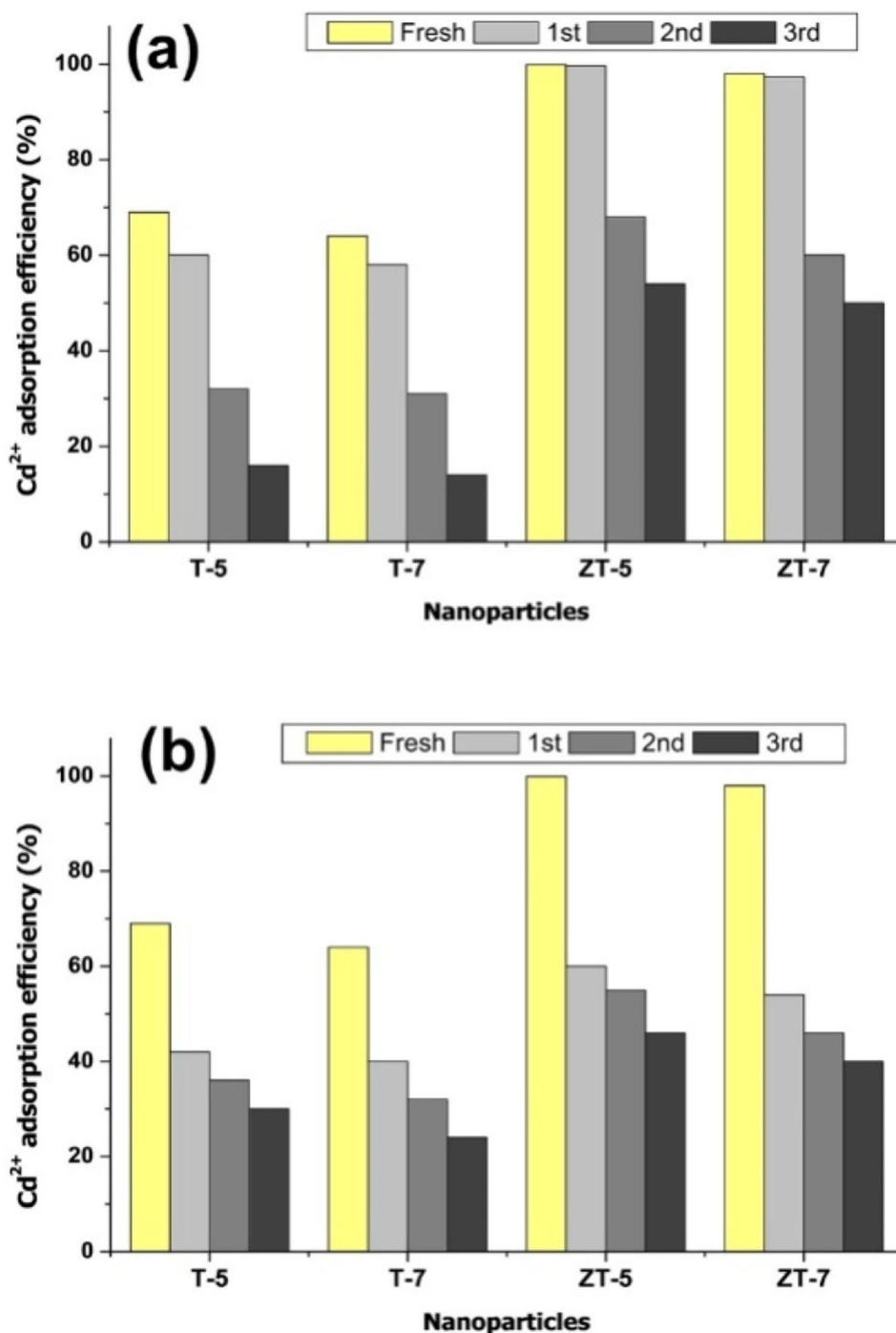
Desorption study

Effective adsorption process depends on the capacity of the adsorbed metal ions on adsorbents, which should not be desorbed easily in ordinary conditions. The desorption study conceded using $CaCl_2$ (0.01 M), where the calcium ion is a leading cation present in water. Calcium cations can replace the adsorbed metals in an aqueous medium that is sorbed by an electrostatic mechanism [1]. The trend of desorption order of zeolite-supported and pure TiO_2 was TiO_2 500 °C (4.2 mg/g) > TiO_2 700 °C (3.5 mg/g) > zeolite-supported 500 °C (1.2 mg/g) > zeolite-supported 700 °C (0.8 mg/g). The maximum desorption value of pure TiO_2 was found high as compared to zeolite-supported TiO_2. Therefore, the zeolite-supported TiO_2 nanoparticles could be worked as stable adsorbents for Cd^{2+} ions.

The unique features of zeolites are very effective to modify the surface properties of TiO_2 (Fig. 10). Zeolite

Fig. 10 The mechanism of Cd^{2+} adsorption and MB degradation on biphasic zeolite-supported TiO_2 nanoparticles
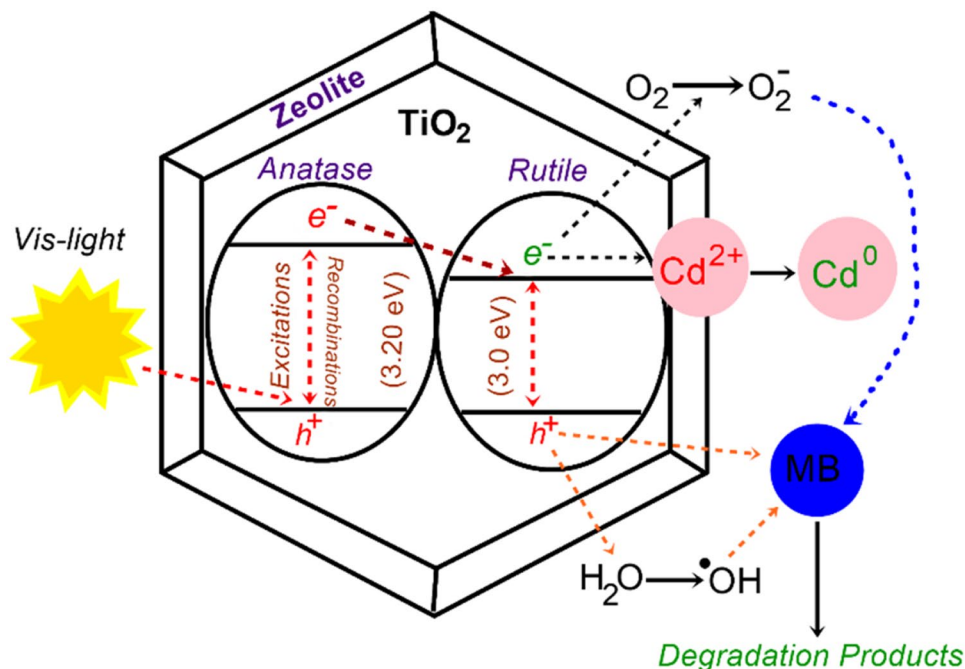
owing distinctive characteristics of such as, (a) chemical, photochemical and thermal inertness and stability, (b) transparency toward UV and visible irradiation, (c) enhanced adsorption efficiency for the pollutants in solution, (d) polarizing strength of surface and inside pores, which balance ion charges during adsorption, and (e) ability of the zeolite structural framework has the electron-donating or accepting ability, which is the contribution of zeolites in electron transfer reactions [22, 47]. The enhanced adsorption capacity of zeolite increases the proximity of pollutants on the surface which can be easily adsorbed or degraded photochemically. Similarly, the Si/Al silica modulus also exerts a stronger impact on the adsorption of various ions on the surface of zeolites and nanocomposites [17]. The present work illustrates that besides the physical and chemical characteristics of zeolite, it also promoted the formation of a biphasic mixture (anatase and rutile/brookite) of TiO_2 (85:15 wt%). The biphasic mixture prolongs the lifetime of photo-generated charges (electron/hole pair) and enhances the efficiencies further as compared to pure anatase (TiO_2).

The synthetic protocol of the liquid impregnation method is advantageous to prepare the TiO_2 and zeolite-supported TiO_2 nanoparticles without the involvement of expansive solvents, material, devices, and energy input. This protocol only involves a magnetic stirrer and furnace for calcination treatment. The mass percentage yield of the end product is found more than 95% using low-cost amorphous titanium (IV) dioxide and crystalline zeolite. The high yield and rapid removal efficiencies significantly increased the usefulness of LI-prepared TiO_2 photocatalyst to be used in bulk for drinking and wastewater treatment processes. The reusability of

zeolite-supported composite after recovering by centrifuging shows that the first physical regeneration has the same efficiency compared to the fresh one, Fig. 9. Moreover, after two consecutive usages, the efficiency of physically regenerated composites reduces gradually.

Conclusions

Zeolite-supported TiO_2 composite was prepared by one-step impregnation method. The photo-induced Cd^{2+} adsorption study illustrated that the zeolite-supported TiO_2 showed higher efficiency under ambient conditions as compared to bare TiO_2. The zeolite-supported TiO_2 composites are significantly effective at pH ~ 4, 6, 8, 10. The high adsorption capability of zeolite concentrates the proximity of Cd^{2+} substrate to the active sites on the surface of the composite. The synergistic effect of organic dye (MB) and Cd^{2+} ions in the competitive adsorption study using as-prepared catalysts further enhanced the efficiency and could be advantageously significant for the wastewater treatment of different ionic strengths. Besides the chemical, photochemical, thermal inertness, and high adsorption capability of the zeolite support, it also increased the biphasic (anatase = 85%, and rutile/brookite = 15%) compositions, which are supposed to be responsible for the enhancement in efficiency further. The physical regeneration of all synthesized samples was found useful for the re-utilization as compared to chemical regeneration. The desorption values of pure TiO_2 were found high as compared to zeolite-supported TiO_2, hence

the zeolite-supported TiO_2 nanoparticles could be worked as stable adsorbents for Cd^{2+} ions.

Compliance with ethical standards

Conflict of interest The authors declare that they have no conflict of interest.

References

1. S. Mahdavi, Clean Technol. Environ. Policy **18**, 817–827 (2016)
2. S. Ashraf, Q. Ali, Z.A. Zahir, S. Ashraf, H.N. Asghar, Ecotoxicol. Environ. Safety **174**, 714 (2019)
3. U.S. EPA, *Exposure Factors Handbook 2011 Edition (Final)* (U.S Environmental Protection Agency, Washington, DC, 2011)
4. M. Trgo, J. Perić, N.V. Medvidović, J. Hazard. Mater. **136**, 938 (2006)
5. M. Mohsen-Nia, P. Montazeri, H. Modarress, Desalination **217**, 276 (2007)
6. P. Pengthamkeerati, T. Satapanajaru, P. Chularuengoaksorn, Fuel **87**, 2469 (2008)
7. A.D. Delil, O. Gülçiçek, N. Gören, Int. J. Environ. Res. **13**, 861 (2019)
8. I. Kula, M. Uğurlu, H. Karaoğlu, A. Celik, Bioresour. Technol. **99**, 492 (2008)
9. S.E. Bailey, T.J. Olin, R.M. Bricka, D.D. Adrian, Water Res. **33**, 2469 (1999)
10. M.R. Abukhadra, M. Shaban, F. Sayed, I. Saad, Environ. Sci. Pollut. Res **25**, 33264 (2018)
11. XXu.X. Cao, L. Zhao, H. Wang, H. Yu, B. Gao, Environ. Sci. Pollut. Res **20**, 358 (2013)
12. L. Foo, C. Tee, N. Raimy, D. Hassell, L. Lee, Clean Technol. Environ. Policy **14**, 273 (2012)
13. M.R. Abukhadra, B.M. Bakry, A. Adlii, S.M. Yakout, M.E. El-Zaidy, J. Hazard. Mater. **374**, 296 (2019)
14. M. Visa, A. Duta, Chem. Eng. J. **223**, 860 (2013)
15. M. Abdel Salam, M.R. Abukhadra, A. Adlii, ACS omega **5**, 2766 (2020)
16. N.U. Saqib, R. Adnan, I. Shah, Mater. Res. Exp. **6**, 095506 (2019)
17. G. Kravchenko, E. Domoroshchina, G. Kuzmicheva, A. Gaynanova, S. Amarantov, L. Pirutko, A. Tsybinsky, N. Sadovskaya, E. Kopylova, Nanotechnol. Russia **11**, 579 (2016)
18. X. Guo, S. Zhang, X.-Q. Shan, J. Hazard. Mater. **151**, 134 (2008)
19. A. Fujishima, X. Zhang, D.A. Tryk, Surf. Sci. Rep. **63**, 515 (2008)
20. V.N.H. Nguyen, R. Amal, D. Beydoun, Chem. Eng. Sci. **58**, 4429 (2003)
21. N.U. Saqib, A. Khan, I. Alam, M. Rahim, SN Appl. Sci. **2**, 619 (2020)
22. R.J. Tayade, R.G. Kulkarni, R.V. Jasra, Ind. Eng. Chem. Res. **46**, 369 (2007)
23. L. Zhao, T. Cui, Y. Li, B. Wang, J. Han, L. Han, Z. Liu, RSC Adv. **5**, 64495 (2015)
24. G. Liu, D. Zhu, S. Liao, L. Ren, J. Cui, W. Zhou, J. Hazard. Mater. **172**, 1424 (2009)
25. S. Izadyar, S. Fatemi, Ind. Eng. Chem. Res. **52**, 10961 (2013)
26. M. Kumar, A.K. Gupta, D. Kumar, Ceram. Int. **42**, 405 (2016)
27. S. Wang, H. Li, S. Xie, S. Liu, L. Xu, Chemosphere **65**, 82 (2006)
28. W. Zhang, X. Xiao, L. Zheng, C. Wan, Appl. Surf. Sci. **358**, 468 (2015)
29. D.C. Hurum, A.G. Agrios, K.A. Gray, T. Rajh, M.C. Thurnauer, J. Phys. Chem. B **107**, 4545 (2003)
30. S. Saha, J. Wang, A. Pal, Sep. Purif. Technol. **89**, 147 (2012)
31. E.M. Hotze, T. Phenrat, G.V. Lowry, J. Environ. Qual. **39**, 1909 (2010)
32. M. Samarghandi, J. Nouri, A. Mesdaghinia, A. Mahvi, S. Nasseri, F. Vaezi, Int. J. Environ. Sci. Technol. **4**, 19 (2007)
33. W. Janusz, M. Matysek, J. Colloid Interface Sci. **296**, 22 (2006)
34. L. Skubal, N. Meshkov, T. Rajh, M. Thurnauer, J. Photochem. Photobiol. A Chem. **148**, 393 (2002)
35. M. Zulfiqar, S. Sufian, N.E. Rabat, N. Mansor, J. Mol. Liquids **308**, 112941 (2020)
36. W. Cheung, Y. Szeto, G. McKay, Bioresour. Technol. **98**, 2897 (2007)
37. S. Sharaf El-Deen, F.-S. Zhang, J. Exp. Nanosci. **11**, 239 (2016)
38. R. Zha, R. Nadimicherla, X. Guo, J. Mater. Chem. A **2**, 13932 (2014)
39. I. Shah, R. Adnan, W.S.W. Ngah, N. Mohamed, Y.H. Taufiq-Yap, Bioresour. Technol. **160**, 52 (2014)
40. M. Islam, R. Patel, J. Hazard. Mater. **143**, 303 (2007)
41. K.E. Engates, H.J. Shipley, Environ. Sci. Pollut. Res. **18**, 386 (2011)
42. E. Unuabonah, K. Adebowale, B. Olu-Owolabi, L. Yang, L. Kong, Hydrometallurgy **93**, 1 (2008)
43. Y.-C. Lee, J.-W. Yang, J. Ind. Eng. Chem. **18**, 1178 (2012)
44. E. Giarratano, M. Faleschini, C. Bruni, N.L. Olivera, M.N. Gil, Int. J. Environ. Res. **13**, 581 (2019)
45. J.H. Roque-Ruiz, E.A. Cabrera-Ontiveros, J. Torres-Pérez, S.Y. Reyes-López, Water Air Soil Pollut. **227**, 286 (2016)
46. A. Usman, A. Sallam, M. Zhang, M. Vithanage, M. Ahmad, A. Al-Farraj, Y.S. Ok, A. Abduljabbar, M. Al-Wabel, Water Air Soil Pollut. **227**, 449 (2016)
47. S. Hashimoto, J. Photochem. Photobiol. C **4**, 19 (2003)